Computers and Chemical Engineering 181 (2024) 108516

Contents lists available at ScienceDirect

Computers and Chemical Engineering

journal homepage: www.elsevier.com/locate/compchemeng

Robust plastic waste classification using wavelet transform multi-resolution analysis and convolutional neural networks

Fei Long [a,1,*], Shengli Jiang [b,1], Ezra Bar-Ziv [a], Victor M. Zavala [b]

[a] Department of Mechanical Engineering, Michigan Technological University, Houghton, MI 49931, USA
[b] Department of Chemical and Biological Engineering, University of Wisconsin-Madison, Madison, WI 53706, USA

ARTICLE INFO

Keywords:
Convolutional neural network
Grad-CAM
Wavelet transform
Mid-infrared spectroscopy
Plastic classification

ABSTRACT

Mid-infrared spectroscopy (MIR) using photon up-conversion provides advantages over near-infrared spectroscopy (NIR) for plastic waste recycling, including comparable data collection speed and the ability to detect black plastics. However, high-speed MIR spectra suffer from the presence of significant noise. While convolutional neural networks (CNNs) have been utilized for accurate classification of noisy MIR spectra, the analysis of extracted features by the CNN has received less attention. In this study, we analyzed features extracted by a CNN from high-speed MIR spectra collected at 200 spectra per second. Visualizing salient features through the Grad-CAM method revealed that, although the CNN model achieved 100% accuracy, the predictions were not reliable or robust, as the model is susceptible to noise interference. To address this limitation, we propose a wavelet transform-based multi-resolution analysis (MRA) as a preprocessing method for noisy MIR spectra. We show that MRA reconstruction effectively captures features related to characteristic IR peaks, enabling the CNN model to extract informative features from noisy MIR spectra and significantly improves the prediction fidelity and robustness.

1. Introduction

Plastic waste is a pressing global issue, both economically and environmentally (EPA 2020). Addressing this problem necessitates an efficient and sophisticated system for recycling plastic waste. This process forms a pipeline that necessitates a sequence of stages such as collection, transportation, sorting, and recovery, as shown in Fig. 1. A great challenge within this recycling chain, particularly prior to the recovery stage, is the task of sorting or classification of plastics. To ensure high-quality and high-value recycled plastic, the waste must be meticulously sorted, segregating different types of plastics in preparation for the recovery process.

To effectively recycle mixed plastic wastes (MPW) on a large scale, fast detection and accurate sorting or classification are crucial. Many waste facilities, including municipal recycling centers and commercial recycling companies, have adopted near-infrared spectroscopy (NIR) technology as a standard practice for their operations. NIR is a non-destructive method for identifying materials based on their molecular structure, making it well-suited for recycling applications where the goal is to separate materials for reuse or further processing. One of the most important advantages of NIR is its high data acquisition speed up to hundreds of spectra per second. However, NIR suffers from the limitations in detecting black plastics (Ragaert et al., 2017; Faraca and Astrup, 2019), which comprise approximately 15% of MPW (Turner, 2018). As a result, most black plastic items end up in our landfills and incinerators, because the NIR used by recycling facilities cannot "see" the color black. A promising alternative to NIR is mid-infrared spectroscopy (MIR) using photon up-conversion technique (Becker et al., 2017), in which photons are transformed from the IR spectral range into the near infrared spectral range and fast silicon detectors can be used. MIR spectroscopy combines the high accuracy of the infrared spectral range with the high speed of NIR. More importantly, MIR spectroscopy can detect black plastics, which can improve the overall recycling efficiency of MPW.

For industrial application purposes, both NIR and MIR spectroscopic data have low signal-to-noise ratio (SNR) due to the fast measurement speed. In addition, the plastic samples are moving on a conveyer belt which introduces more sources of noise due to the vibration and disturbance. To accurately classify the noisy spectra, many convolutional neural network (CNN) models have been developed (Jiang et al., 2021; Zinchik et al., 2021; Michel et al., 2020; Zhu et al., 2019). CNN is a

* Corresponding author.
E-mail address: flong@mtu.edu (F. Long).
[1] Fei Long and Shengli Jiang contributed equally to this paper.

https://doi.org/10.1016/j.compchemeng.2023.108516
Received 24 July 2023; Received in revised form 28 October 2023; Accepted 19 November 2023
Available online 24 November 2023

type of deep learning method that can automatically learn to extract distributed features of input data. The primary advantage of CNN is that it provides automatic feature extraction by loads of convolutional and pooling layer pairs (Liu et al., 2021). Despite the tremendous success, the non-linear nature of these models as well as the noise and other sources of variability in the spectra make it difficult to extract meaningful information. To alleviate concerns regarding the fidelity of data-driven model predictions, various preprocessing methods have been developed to improve the quality of IR spectra and enhance their interpretability (Guillemé et al., 2019; Pandey et al., 2022). Wavelet analysis has emerged as a promising approach for preprocessing spectroscopic data. Wavelet analysis is a mathematical technique used to break down a signal into various frequency components, enabling a comprehensive analysis of the signal across multiple scales. In the realm of IR spectroscopy, wavelet analysis proves beneficial by eliminating noise and other sources of variability from spectra (Shabani et al., 2018; Chen and Lu, 2022). The main advantage of wavelet analysis compared with other noise-filtering methods is the possibility of localizing the frequency information to selected parts of the data. In IR spectra, complex characteristic peaks are located at different regions with different shapes. Fourier Transform (FT) or smoothing window denoising methods apply a single cut-off frequency for all peaks, which may either include too much noise or filter out important peaks. Wavelet analysis outperforms in such cases because it is localized in both the wavelength and frequency domains. This process enhances the quality of the spectra, facilitating the extraction of meaningful features (Alsberg and B, 1997; Xie et al., 2017; Raczkowska et al., 2019; Trevisan et al., 2012; Lu et al., 2020).

In this study, we investigate the effectiveness of wavelet transform-based MRA for preprocessing noisy MIR spectra. We compare the MIR features extracted by a CNN model with and without MRA preprocessing and visualize them using Grad-CAM (Selvaraju et al., 2019). Without preprocessing, the CNN achieves nearly 100% classification accuracy on test spectra, but the predictions are not based on the characteristic IR peaks of the plastics. In contrast, with the wavelet-based preprocessing, CNN successfully identifies the characteristic IR peaks and achieves 100% classification accuracy based on these features. Our results demonstrate that MRA preprocessing improves CNN feature selection, leading to a more explainable machine learning model with enhanced fidelity and robustness.

2. Experimental data collection

2.1. MIR measuring system

The schematic experimental setup is shown in Fig. 2. The IR source (a 1000 °C silicon nitride, Si_3N_4 light source, 4.5 mm in diameter and 17 mm long, heated by 70 W electric power, Hawkeye Technologies model IR-Si311) was placed at the focus of an aluminum elliptical reflector which focused the light at 200 mm from the front surface of the reflector, projecting the light on a gold diffuser, generating a circular area with

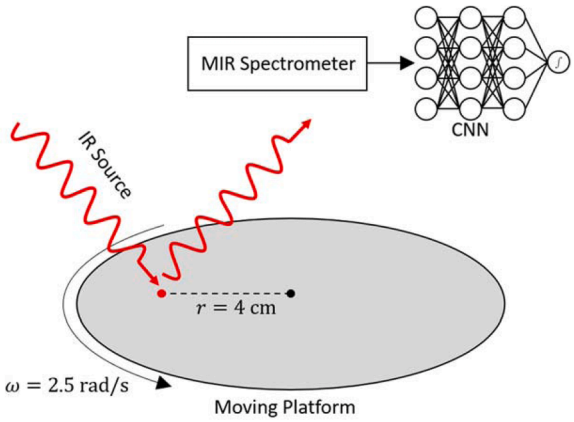

Fig. 2. Experimental setup. The plastic samples are placed on the moving platform to mimic the industrial application.

around 10 mm diameter. Some of the reflected light from the plastic surface was collected by a 1 in. parabolic gold-coated aluminum mirror (with a focal length of 200 mm) that collimated light from the diffuser, after which a 40 mm CaF_2 lens focused the light into a 200 μm core indium fluoride (InF3) fiber that was connected to an MIR spectrometer (NLIR S2050, Denmark). In our previous work (Jiang et al., 2021), we provided detailed information about the up-conversion MIR spectrometer. Briefly, spectrometer (NLIR S2050) is based on sum-frequency generation in a $\chi(2)$-nonlinear $LiNbO_3$ crystal that upconverts MIR light from the band $2.0 - 5.0$ μm to the near-visible region 695−877 nm (Barh et al., 2017; Friis and Høgstedt, 2019; Jahromi et al., 2019; Meng et al., 2018). The upconversion spectrometer offers several advantages, including the exclusion of most thermal noise (Pedersen et al., 2018) and the utilization of silicon-based CMOS array detectors that exhibit superior detectivities compared to traditional MIR detectors such as HgCdTe (MCT) or PbSe array detectors. The CMOS detector comprises 2048 pixels, and the spectral resolution is <6 cm^{-1}.

To replicate the conveyor belt in an industrial setting, the plastic samples were placed on a moving platform. This platform was operated by a 12 V DC motor, with an angular velocity set at 2.5 rad/s. The MIR source was positioned at a fixed focal point, located 40 mm away from the center of the platform. This distance corresponded to a linear speed of 100 mm/s of the samples. The platform surface was made of urethane, a common material used for conveyor belts in industrial applications.

2.2. Spectroscopic data collection

In this study, we focused on 5 commercially available plastic materials commonly found in mixed plastic waste (MPW): black polystyrene (PS), black polyethylene (PE), deep blue polypropylene (PP), white polyvinyl chloride (PVC) and black polycarbonate (PC). These plastic samples were 1 mm thick sheets obtained from ePlastics (San Diego,

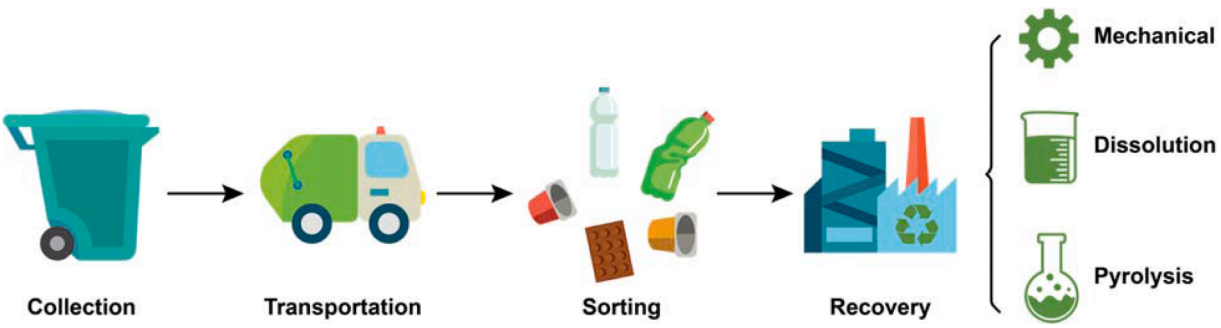

Fig. 1. A common workflow for mixed plastic waste recycling. Accurate and high-throughput sorting is an important step for subsequent recovery phases.

California, United States). In addition, we also considered the black urethane, which is a common conveyer belt material, referred to as the background (BK) in the following context. The plastic sheets were cut to match the size of the platform and MIR spectra were collected by placing the samples on the moving platform to include vibration noise. We selected 900 data points in each spectrum within the wavenumber range of 2350 cm^{-1} to 3950 cm^{-1} for the wavelet analysis and machine learning classification. For each sample, 1000 spectra were collected at a measurement rate of 200 spectra per second, resulting in a total of 6000 spectra.

The 20 randomly selected spectra of each sample are shown in Fig. 3. PE and PP exhibit discernible characteristic peaks within the 2900 cm^{-1} to 3000 cm^{-1} range attributed to C-H stretching. The peaks in the remaining samples are obscured by noise. Furthermore, PC, PS and PVC demonstrate closely resembling spectral patterns, which makes it challenging for accurate and robust classification.

3. Wavelet preprocessing and CNN

3.1. Multiresolution analysis

In the realm of signal processing and image analysis, the wavelet transform serves as a pivotal mathematical instrument. Its significance is particularly highlighted in the field of multiresolution analysis (MRA), a complex yet profoundly insightful process which fractionates a signal into multiple constitutive elements. These segmented parts, when combined, precisely reconstruct the original signal. By decomposing the inherent variability of the data, the wavelet transform elucidates the underlying structures and makes it feasible to interpret the data in physically meaningful ways. An in-depth exploration of the theoretical foundation and the comprehensive mathematical description of the wavelet transform can be found in the literature (Alsberg et al., 1997). Briefly, a wavelet can be defined as a function of the following form:

$$\psi_{a,b}(t) = \frac{1}{\sqrt{a}}\psi\left(\frac{t-b}{a}\right) \quad a, b \in \mathbb{R} \tag{1}$$

where a and b are called *scale* and *position* parameters, respectively. The functional form, $\psi_{a,b}(t)$, represents a waveform of effectively limited duration which is characterized by an average value of zero. The scale parameter a defines the width of the wavelet duration, and the position parameter b determines the position where the wavelet convolutes with the original signal.

For a particular signal denoted by $f(t)$, the coefficients of the wavelet transform corresponding to a given scale a can be computed as:

$$wt(a,b) = \int_{-\infty}^{+\infty} f(t)\cdot\psi_{a,b}(t)\mathrm{d}t \tag{2}$$

In its operation, the wavelet transforms capture high-frequency information from $f(t)$ at lower scale values a, similar to adjusting the resolution of a microscope. This attribute of the wavelet transform empowers it to dissect information across different resolution levels, bringing forth valuable insights concealed within original data.

Fig. 4(a) shows a randomly selected PE spectrum, the inset is the Daubechies 4 wavelet (db2 wavelet) used for the decomposition. The selection of db2 wavelet was primarily due to its morphological similarity to the peaks observed in MIR spectra, thereby enhancing the capability of feature extraction.

Fig. 4(b) delineates the coefficients corresponding to eight levels of

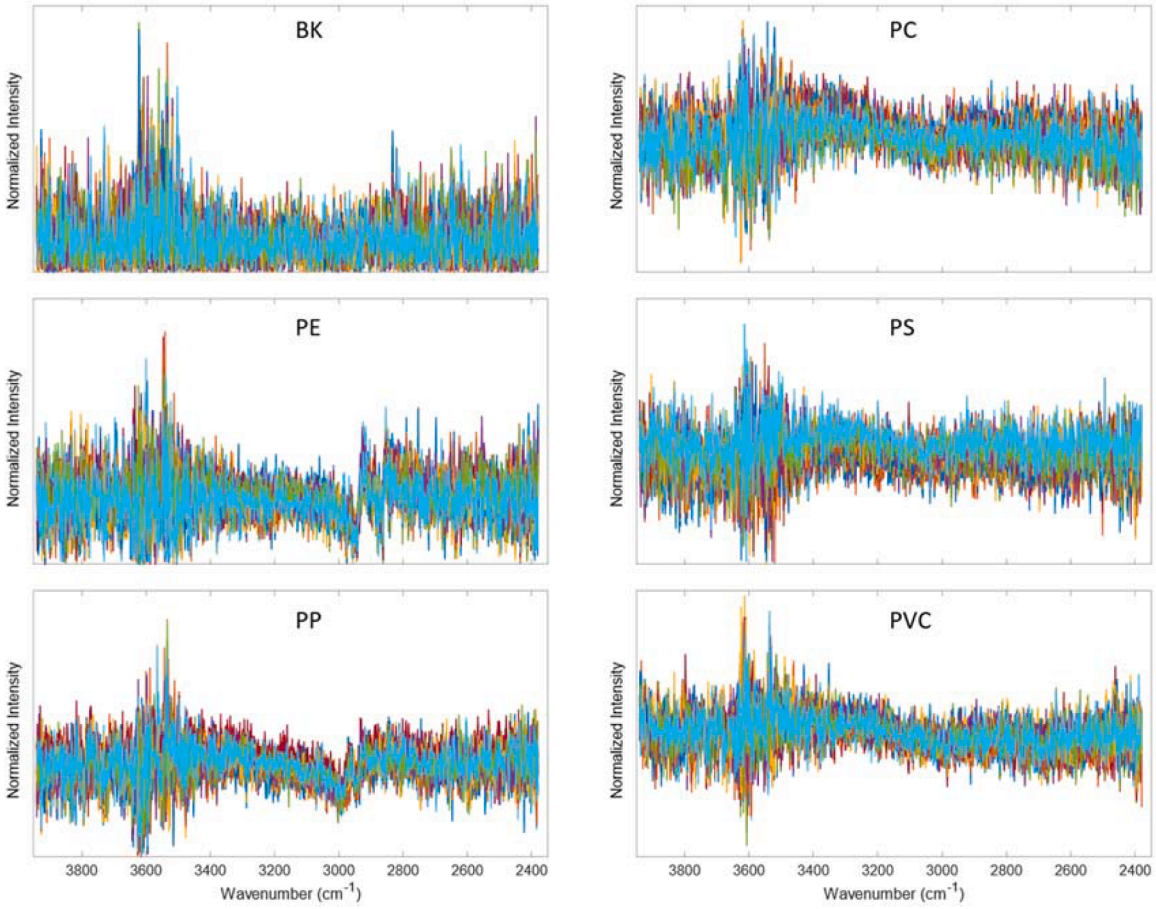

Fig. 3. MIR spectra measured at the rate of 200 spectra per second. 20 randomly selected spectra of each sample are plotted.

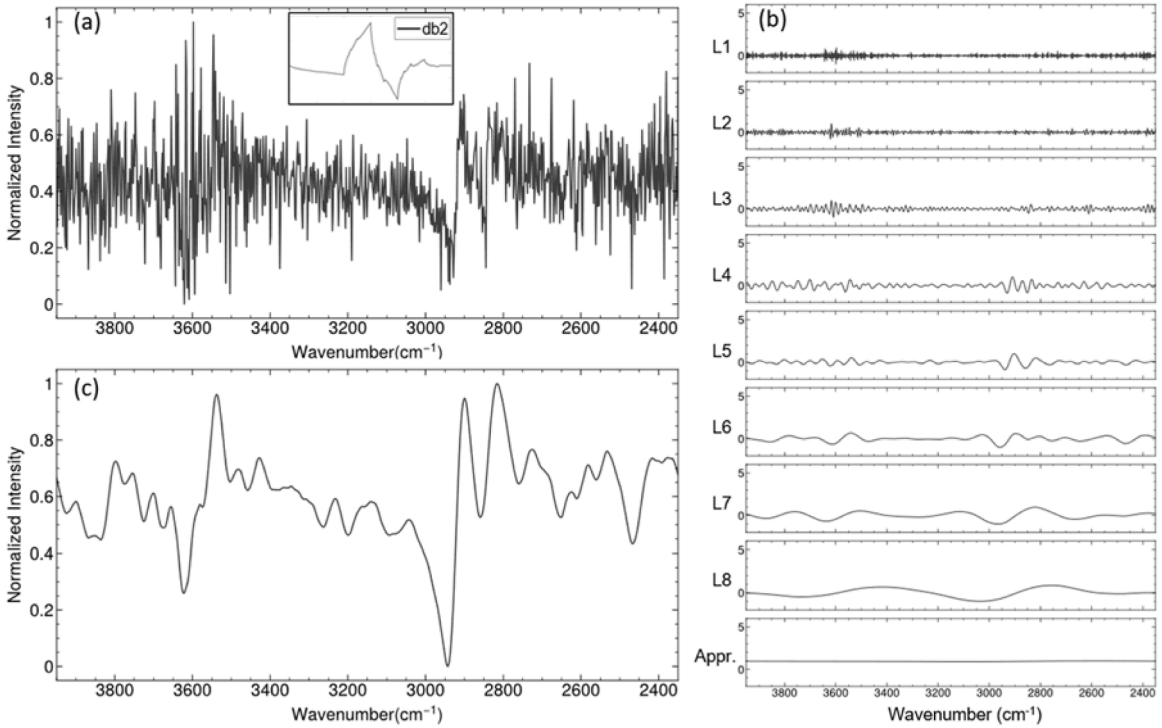

Fig. 4. (a) MIR spectra of PE. The inset shows the 'db2' wavelet function used for the decomposition. (b) MRA Coefficients of 8 level decomposition from L1 to L8, as well as the approximation (Appr.) (c) Reconstructed spectrum by summing the components in (b) from L5 to L8.

decomposition, ranging from L1 to L8. It also includes an additional representation of the approximation (Appr.) coefficients. The L1 level captures the highest frequency information, while the approximation coefficient embodies the lowest frequency information, effectively representing the baseline trend in the spectrum.

After the decomposition, we reconstructed the spectrum by summing the coefficients from L5 to L8. This reconstruction process effectively eliminated the high frequency components and removed the baseline. As depicted in Fig. 4(c), the reconstructed spectrum effectively reduces noise while enhancing the characteristic IR peaks. The reconstructed spectra of other plastic samples are presented in Fig. S1. Both the raw spectra and the reconstructed spectra were normalized before the machine learning training and classification.

When juxtaposed with popular low-pass filter denoising, the wavelet transform has clear advantages. It allows for multiresolution analysis, capturing both high and low-frequency details, whereas low-pass filters might miss such nuances. Furthermore, wavelets are inherently localized in both wavelength and frequency, enabling precise noise removal especially when noise varies across the signal. In contrast, low-pass filters operate globally, potentially missing localized signal characteristics.

3.2. CNN model

The reconstructed MIR spectra were analyzed with a 1D CNN. The architecture of the proposed 1D CNN is shown in Fig. 5. The 1D CNN, employing both convolution and pooling methods, extracts important features from the reconstructed MIR spectra. Each convolutional filter in our design is represented as a 3D vector. The convolved signal, which is a scalar value, signifies the presence (high value) or absence (low value) of the pattern the filter aims to detect. Convolutional operations then perform a nonlinear transformation (e.g., rectified linear units) to transform one vector into another of identical dimension. These filters are referred to as convolutional layers. Convolutional operations substantially augment the information to be processed. Hence, it becomes essential to summarize this information. To achieve this, we apply a max-pooling operation to diminish the dimension, taking a portion of a given vector (specifically, a size 2 subset in our model) and reduces it to a single value by extracting the maximum value. This effectively reduces the vector dimensions emerging from the convolutional layer, distilling the important information.

The 900 datapoints reconstructed MIR spectra were fed into the 1D CNN. The first two convolutional layers contained 32 filters with a size of 7 each. The third convolutional layer comprised 64 filters, each of size

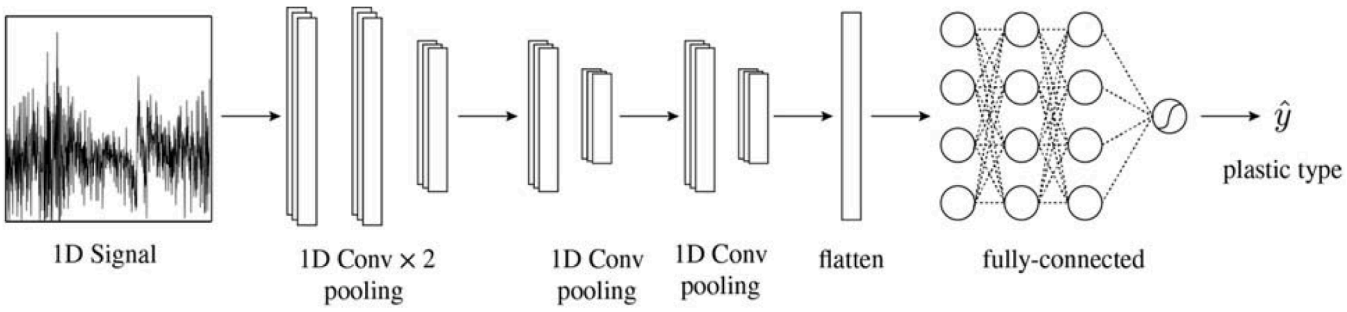

Fig. 5. The architecture of the proposed 1D CNN.

7, and the fourth convolutional layer had 128 filters of size 7. Each fully connected layer incorporated 128 nodes, and every max-pooling layer utilized a filter of size 2. Between the layers, Rectified linear units (ReLUs) functioned as activation functions. A dropout ratio of 0.2 was introduced between each pair of fully connected layers to mitigate overfitting. The output layer operated with the softmax activation function, and categorical cross-entropy served as the loss function. The output vector, having a dimension of 6, signified the probability that the MIR spectra derived from a specific plastic type. The convolutional layers and max-pooling layers were organized recursively in 1D CNN to extract information at both the local and global scales. In addition, this arrangement facilitated the condensation of data essential for the classification of the corresponding type of plastic.

We leveraged a 5-fold cross-validation strategy to ensure the reliability of our CNN model. Initially, we evenly split the dataset into five random subsets. During each cross-validation iteration, we dedicated one subset (20% of the total data) to testing, and the remaining four subsets (80%) to model training. This five-fold procedure assured each subset was used as test data exactly once, enabling a comprehensive model evaluation across diverse data sections. To ensure homogeneity in each subset before sampling, we applied stratification, maintaining an equivalent proportion (16.7%) of each plastic type in the training and testing sets.

The training data was further divided, allocating 75% for model training and 25% for validation. This division resulted in 3600 training, 1200 validation, and 1200 testing samples per fold. The final accuracy, computed as the mean accuracy over the five folds, represents the overall performance of the model and its generalizability.

The data and codes can be found at: https://github.com/zavalab/ML/tree/master/Plastic_Wavelet.

3.3. Grad-CAM

In this study, the Gradient-weighted Class Activation Mapping (Grad-CAM) (Selvaraju et al., 2019) method is employed to augment the interpretability of CNNs. Its implementation does not affect the classification performance of CNNs. It achieves this by visualizing the regions of focus during the classification process. A heat map is generated, overlaying the input, and highlighting important regions involved in classification. The essence of Grad-CAM lies in its usage of the gradients of the output label, i.e., types of plastic, directed into the final convolutional layer to generate a saliency map, which emphasizes the significant regions in the IR spectral input.

The Grad-CAM algorithm is applied as follows:

1. The final convolutional layer consists of $K = 128$ output channels, each resulting in a feature map vector represented by $\boldsymbol{a}^k \in \mathbb{R}^{225}$, for $k = 1, \cdots, 128$
2. After model training, the gradients of the output probability for true plastic type c, y^c, relative to the feature map vector $\boldsymbol{a}^k$ are calculated.
3. The gradients are then averaged to derive the importance weights (ω_k^c) using the formula:

$$\omega_k^c = \frac{1}{N}\sum_i \frac{\partial y^c}{\partial \boldsymbol{a}_i^k} \tag{3}$$

where $N = 225$ is the dimension of the feature map vector. These weights reflect the importance of feature map vector k for a target plastic type c.

4. The final step involves linearly combining the feature map vectors weighted by these importance weights, followed by a ReLU activation, to generate the Grad-CAM saliency map $\mathscr{S}^c \in \mathbb{R}^{225}$:

$$\mathscr{S}^c = \mathrm{ReLU}\left(\sum_k \omega_k^c \boldsymbol{a}^k\right) \tag{4}$$

ReLU activation ensures that we only consider features that have a positive impact on the relevant plastic type, thus effectively removing negative entries that may have a high impact on other plastic types.

Due to the downscaling in convolutional and pooling layers, the Grad-CAM saliency map, denoted as $\mathscr{S}^c$, typically has a smaller dimension than the input. To visualize important regions in the input spectra, interpolation techniques are employed for upsampling. The default "antialiased" interpolation method from the Python Matplotlib package is used for this purpose.

Given the implementation of 5-fold cross-validation in training the CNN models, we computed Grad-CAM for each model corresponding to each fold. Subsequently, we derived an average saliency map $\mathscr{S}^c_{\mathrm{avg}}$, aggregating the results across all models as shown in Fig. 8.

4. Results and discussion

4.1. Principal component analysis

To investigate the direct impact of MRA, we employed principal component analysis (PCA) on both the raw and MRA reconstructed spectra. The first two principal components of each spectrum are visually represented in Fig. 6. In the inspection of the raw spectra, we found three distinct clusters, corresponding to PE, PP, and BK samples. However, these clusters were notably compact. On the other hand, the PC, PS, and PVC samples displayed an overlapping pattern, highlighting spectral similarities and complicating their differentiation using CNN. For the MRA reconstructed spectra, the distinct clusters corresponding to PE, PP, and BK maintained their isolation but with a marked expansion, indicating a more extensive distribution. Additionally, PC, PS, and PVC samples still had an overlapping pattern, but with larger cluster sizes.

The compact clustering observed in the raw spectra could be ascribed to measurement-dependent features such as baseline trends. These factors may enable precise predictions within a single measurement batch, yet potentially compromise generalizability to future applications due to potential baseline variations. By minimizing these measurement-dependent factors through MRA, the reconstructed spectra exhibited larger, well-regularized clusters.

The spread of PC clusters suggests that the variability of random noises within high-throughput measurements is effectively captured. Despite this, the overlapping of PC, PS, and PVC samples remained observable, indicating that inherent spectral similarities persist, even after MRA reconstruction.

4.2. Convolutional neural network classification

The CNN models were trained utilizing both raw and MRA-reconstructed spectra. Notably, overlapping clusters were observed in the PC, PS, and PVC samples in Fig. 6, potentially complicating classification. Nevertheless, both datasets produced near 100 % prediction accuracies. The confusion matrices of the test datasets are shown in Fig. 7. Despite the high prediction accuracy, the robustness of the CNN model depends on the features extracted by the convolutional layers. When classifying the infrared spectroscopic data, it is essential that the features are directly related to the characteristic absorption peaks.

4.3. Grad-CAM feature analysis

We utilized Grad-CAM to investigate the salient features extracted by the CNN models from each data set, with the corresponding heatmaps presented in Fig. 8. In general, the raw spectra resulted in the extraction of a larger number of features, which were observed to be dispersed and manifested as narrow bands in the generated heatmaps, as shown in

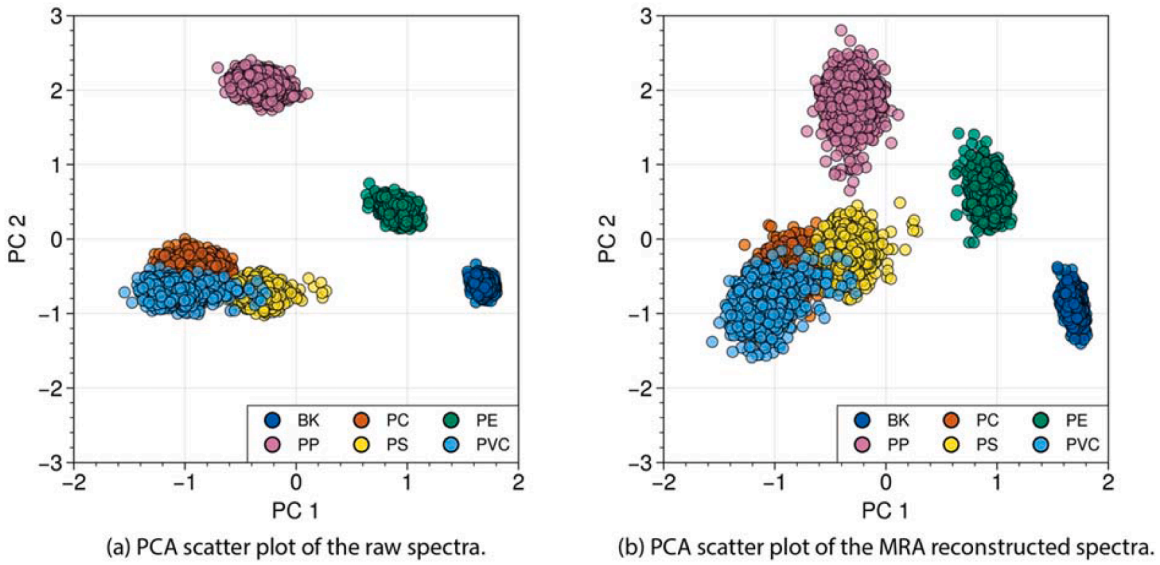

Fig. 6. Scatter plots of the first and second principal components of (a) the raw spectra and (b) the MRA reconstructed spectra.

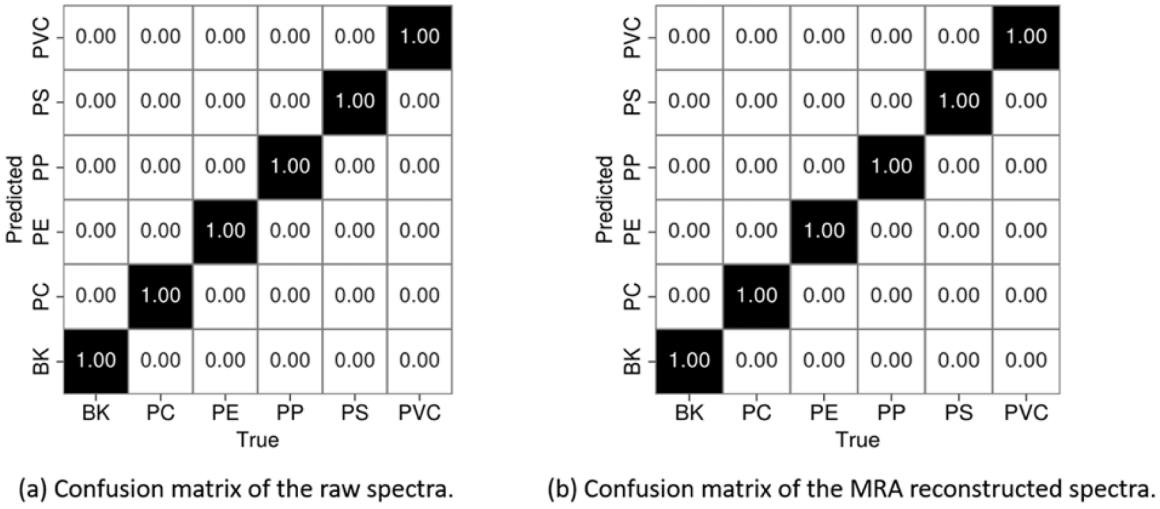

Fig. 7. The confusion matrices of the proposed 1D CNN on the test datasets of (a) the raw spectra and (b) the MRA reconstructed spectra.

Fig. 8(a). This may render the CNN model more susceptible to noise interference. Furthermore, when examining PC, PS, and PVC in Fig. 8(a), it was observed that these samples exhibited a scarcity of features within the wavenumber range of 2600 cm^{-1} to 3400 cm^{-1}, which corresponds to the range where the characteristic peaks of these polymers exist. This observation suggests that the CNN model struggled to extract the characteristic IR peak information from the raw data. Consequently, despite achieving 100 % prediction accuracy on the raw spectra, the reliability of CNN predictions is compromised in the absence of features directly related to the crucial characteristic IR peak information.

Conversely, the datasets reconstructed with MRA exhibited a reduced but more concentrated set of features, visualized as denser and more focused color bands within the heatmaps, as shown in Fig. 8(b). Moreover, a subset of the features extracted through wavelet analysis directly corresponded to the characteristic peaks associated with the plastic samples. For example, in the MRA reconstructed BK (urethane) spectrum, while the peaks centered around 3000 cm^{-1} and 3400 cm^{-1} may appear inconspicuous, they are indeed attributed to the stretching vibrations of C-H and N-H bonds, respectively.

Remarkably, the CNN model successfully recognized and assigned substantial importance to these features, leveraging them as influential factors in making accurate predictions. For the MRA reconstructed PC, several features were extracted between 3200 cm^{-1} to 3500 cm^{-1} corresponding to the broad peak of OH stretch. And there was another feature around 3000 cm^{-1} due to C-H stretch. For PE, the features around 2900 cm^{-1} and 2850 cm^{-1} are associated with the CH_2 asymmetric C-H stretch and CH_2 symmetric C-H stretch, respectively. Similarly, in the PP spectrum, multiple peaks around 2850 cm^{-1} are selected as features relating to CH_3 and CH_2 asymmetric and symmetric stretches. For PVC, the CH_2 stretch around 3000 cm^{-1} is also correctly identified as an important feature. The only exception is PS, there is one light band shown around 2900 cm^{-1}, and most of the significant features are in the range of 3200 cm^{-1} to 3700 cm^{-1}, indicating the existence of hydroxyl. The hydroxyl may have come from ambient humidity during the experiment. Similar hydroxyl features can also be observed in the PP spectrum.

Our investigation of the CNN models trained with raw and MRA reconstructed spectra revealed notable differences in the extracted features. While the raw spectra exhibited a larger number of dispersed features, leading to high prediction accuracy, these features did not align with the characteristic IR peaks of the plastic samples. Therefore, prediction accuracy was susceptible to noises and disturbances,

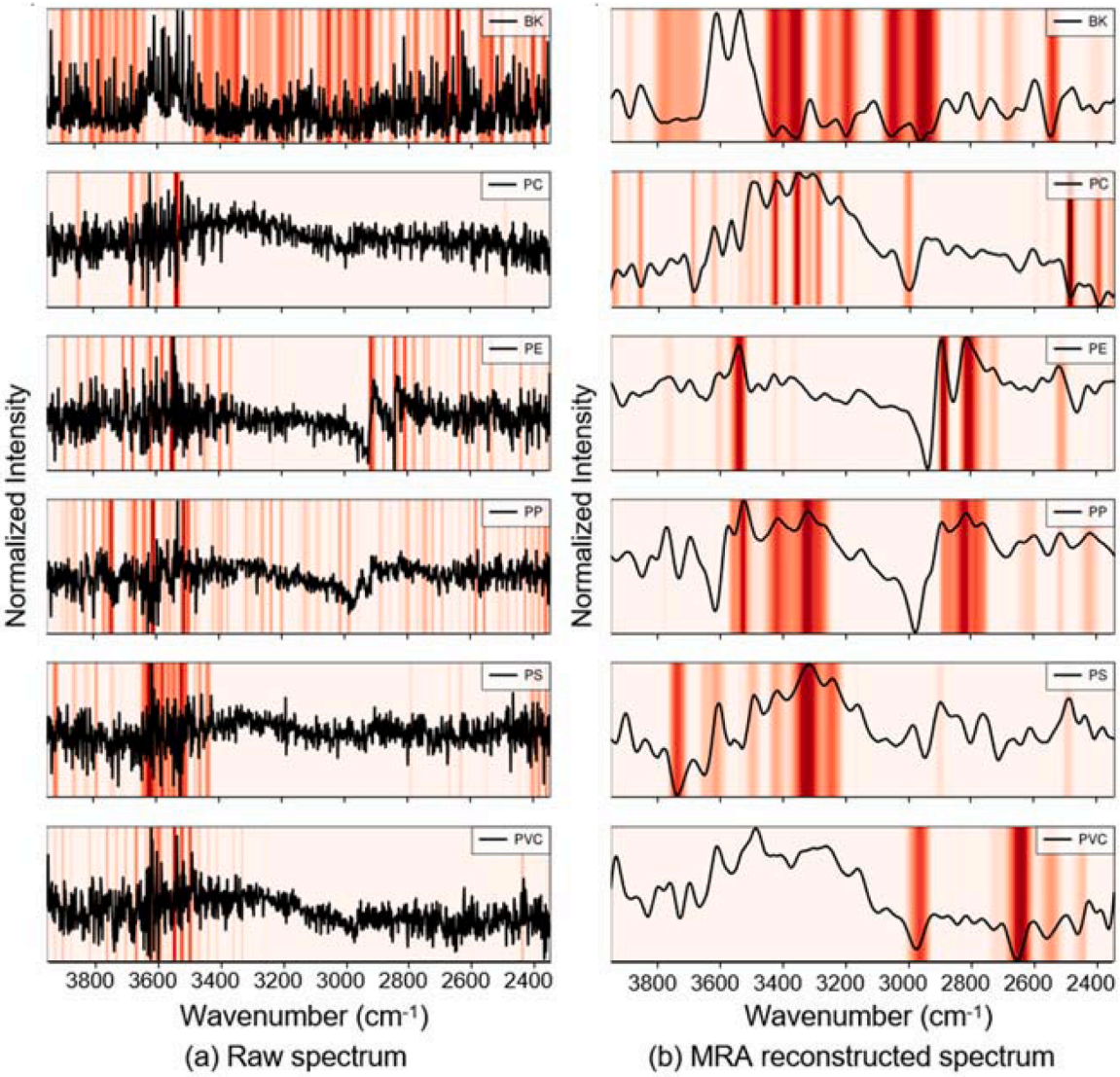

Fig. 8. Heatmap of the salient features extracted from (a) the raw spectra of each plastic sample and (b) the MRA reconstructed spectra of each sample. One randomly selected spectrum of each data set is overlayed on the heatmap to correlate the features with the spectrum.

resulting in a less robust model for future applications. On the other hand, with the help of MRA preprocessing, both the high frequency noise and the low frequency trend were removed from the spectra. The MRA reconstructed datasets displayed a more focused set of features, directly corresponding to the characteristic peaks associated with the plastics. The CNN models successfully identified and prioritized these informative features, resulting in not only accurate but also robust and reliable predictions. In summary, The MRA preprocessing method proved effective in enhancing CNN feature selection towards a more explainable model and can improve the fidelity and robustness of CNN prediction.

5. Conclusions

In this study, we utilized Grad-CAM visualization to investigate the features extracted by CNN model with both the raw MIR spectra and MRA reconstructed spectra. The results demonstrated that MRA serves as an effective preprocessing technique for noisy MIR spectra by removing the high frequency noise and low frequency trend while keeping all the important spectroscopic information. It significantly aids the CNN model in extracting informative features associated with the characteristic IR peaks of the plastic samples. This improves the fidelity and robustness of the CNN-based predictions. In future work, we plan to further assess the robustness of our model in the face of noise variations stemming from alterations in conveyor speeds, temperature, and humidity.

CRediT authorship contribution statement

Fei Long: Methodology, Formal analysis, Software, Writing – original draft, Visualization. **Shengli Jiang:** Methodology, Formal analysis, Software, Writing – original draft, Visualization. **Ezra Bar-Ziv:** Conceptualization, Supervision, Writing – review & editing, Funding acquisition. **Victor M. Zavala:** Conceptualization, Supervision, Writing – review & editing, Funding acquisition.

Declaration of Competing Interest

The authors declare that they have no known competing financial interests or personal relationships that could have appeared to influence the work reported in this paper.

Data availability

Link embedded

Acknowledgments

E.B.-Z. acknowledges funding from U.S. National Science Foundation (NSF) under: (i) PFI-RP-182736 and from (ii) GOALI-203366, and (iii) PFI-RP-2234450.

We acknowledge financial support from the US National Science Foundation under grants IIS-1837812 and 1837821.

Supplementary materials

Supplementary material associated with this article can be found, in the online version, at doi:10.1016/j.compchemeng.2023.108516.

References

Alsberg, B.K., et al., 1997. Wavelet denoising of infrared spectra. Analyst 122 (7), 645–652.
Barh, A., Pedersen, C., Tidemand-Lichtenberg, P., 2017. Ultra-broadband mid-wave-IR upconversion detection. Opt. Lett. 42 (8), 1504–1507.
Becker, W., Sachsenheimer, K., Klemenz, M., 2017. Detection of black plastics in the middle infrared spectrum (MIR) using photon up-conversion technique for polymer recycling purposes. Polymers 9 (9), 435 (Basel).
Chen, J., Lu, X., 2022. How to resolve the maximum valuable information in complex NIR signal: a practicable method based on wavelet transform. Front. Chem. 10.
EPA, 2020. Advancing Sustainable Materials Management: 2018 Fact Sheet Assessing Trends in Material Generation and Management in the United States. United States Environmental Protection Agency Research Triangle Park, Durham, NC.
Faraca, G., Astrup, T., 2019. Plastic waste from recycling centres: characterisation and evaluation of plastic recyclability. Waste Manag. 95, 388–398.
Friis, S.M.M., Høgstedt, L., 2019. Upconversion-based mid-infrared spectrometer using intra-cavity LiNbO3 crystals with chirped poling structure. Opt Lett 44 (17), 4231–4234.
Guillemé, M., et al., 2019. Agnostic local explanation for time series classification. In: Proceedings of the 2019 IEEE 31st International Conference on Tools with Artificial Intelligence (ICTAI).
Jahromi, K.E., et al., 2019. Mid-infrared supercontinuum-based upconversion detection for trace gas sensing. Opt. Express 27 (17), 24469–24480.
Jiang, S., et al., 2021. Using ATR-FTIR spectra and convolutional neural networks for characterizing mixed plastic waste. Comput. Chem. Eng. 155, 107547.
Liu, Y., Pu, H., Sun, D.W., 2021. Efficient extraction of deep image features using convolutional neural network (CNN) for applications in detecting and analysing complex food matrices. Trends Food Sci. Technol. 113, 193–204.
Lu, P., et al., 2020. Accuracy improvement of quantitative LIBS analysis of coal properties using a hybrid model based on a wavelet threshold de-noising and feature selection method. Appl. Opt. 59 (22), 6443–6451.
Meng, L., et al., 2018. Enhancing the detectivity of an upconversion single-photon detector by spatial filtering of upconverted parametric fluorescence. Opt. Express 26 (19), 24712–24722.
Michel, A.P.M., et al., 2020. Rapid identification of marine plastic debris via spectroscopic techniques and machine learning classifiers. Environ. Sci. Technol. 54 (17), 10630–10637.
Pandey, P., Rai, A., Mitra, M., 2022. Explainable 1-D convolutional neural network for damage detection using Lamb wave. Mech. Syst. Signal Process. 164, 108220.
Pedersen, R.L., Hot, D., Li, Z., 2018. Comparison of an InSb detector and upconversion detector for infrared polarization spectroscopy. Appl. Spectrosc. 72 (5), 793–797.
Raczkowska, M.K., et al., 2019. Influence of denoising on classification results in the context of hyperspectral data: high definition FT-IR imaging. Anal. Chim. Acta 1085, 39–47.
Ragaert, K., Delva, L., Van Geem, K., 2017. Mechanical and chemical recycling of solid plastic waste. Waste Manag. 69, 24–58.
Selvaraju, R.R., et al., 2019. Grad-CAM: Visual Explanations from Deep Networks Via Gradient-based Localization. Cornell University Library, Ithaca arXiv.org.
Shabani, Z., Sabouri, S.Ghavami, Khorsandi, A., 2018. Combination of discrete wavelet transform and ANFIS for post processing of spectroscopic signals. Opt. Quantum Electron. 50 (10), 359.
Trevisan, J., et al., 2012. Extracting biological information with computational analysis of Fourier-transform infrared (FTIR) biospectroscopy datasets: current practices to future perspectives. Analyst 137 (14), 3202–3215.
Turner, A., 2018. Black plastics: linear and circular economies, hazardous additives and marine pollution. Environ. Int. 117, 308–318.
Xie, S., et al., 2017. Accuracy improvement of quantitative LIBS analysis using wavelet threshold de-noising. J. Anal. At. Spectrom. 32 (3), 629–637.
Zhu, S., et al., 2019. Plastic solid waste identification system based on near infrared spectroscopy in combination with support vector machine. Adv. Ind. Eng. Polym. Res. 2 (2), 77–81.
Zinchik, S., et al., 2021. Accurate characterization of mixed plastic waste using machine learning and fast infrared spectroscopy. ACS Sustain. Chem. Eng. 9 (42), 14143–14151.